25635579

OUTER RETINAL TUBULATION IN ADVANCED AGE-RELATED MACULAR DEGENERATION

Optical Coherence Tomographic Findings Correspond to Histology

KAREN B. SCHAAL, MD,* K. BAILEY FREUND, MD,* KATIE M. LITTS, BS,†‡ YUHUA ZHANG, PHD,† JEFFREY D. MESSINGER, DC,† CHRISTINE A. CURCIO, PHD†

Purpose: To compare optical coherence tomography (OCT) and histology of outer retinal tubulation (ORT) secondary to advanced age-related macular degeneration in patients and in postmortem specimens, with particular attention to the basis of the hyperreflective border of ORT.

Method: A private referral practice (imaging) and an academic research laboratory (histology) collaborated on two retrospective case series. High-resolution OCT raster scans of 43 eyes (34 patients) manifesting ORT secondary to advanced age-related macular degeneration were compared to high-resolution histologic sections through the fovea and superior perifovea of donor eyes (13 atrophic age-related macular degeneration and 40 neovascular age-related macular degeneration) preserved ≤4 hours after death.

Results: Outer retinal tubulation seen on OCT correlated with histologic findings of tubular structures consisted largely of cones lacking outer segments and lacking inner segments. Four phases of cone degeneration were histologically distinguishable in ORT lumenal walls, nascent, mature, degenerate, and end stage (inner segments and outer segments, inner segments only, no inner segments, and no photoreceptors and only Müller cells forming external limiting membrane, respectively). Mitochondria, which are normally long and bundled within inner segment ellipsoids, were small and scattered within shrunken inner segments and cell bodies of surviving cones. A lumenal border was delimited by an external limiting membrane. Outer retinal tubulation observed in closed and open configurations was distinguishable from cysts and photoreceptor islands on both OCT and histology. Hyperreflective lumenal material seen on OCT represents trapped retinal pigment epithelium and nonretinal pigment epithelium cells.

Conclusion: The defining OCT features of ORT are location in the outer nuclear layer, a hyperreflective band differentiating it from cysts, and retinal pigment epithelium that is either dysmorphic or absent. Histologic and OCT findings of outer retinal tubulation corresponded in regard to composition, location, shape, and stages of formation. The reflectivity of ORT lumenal walls on OCT apparently does not require an outer segment or an inner/outer segment junction, indicating an independent reflectivity source, possibly mitochondria, in the inner segments.

RETINA 0:1–12, 2015

Outer retinal tubulation (ORT) was first described histologically as interconnecting tubes containing degenerate photoreceptors and enveloping Müller cells in age-related macular degeneration (AMD).[1] Carbonic anhydrase histochemistry revealed that ORT is consisted primarily of red-green cones.[1] Processes of Müller cells, normally interleaved between the photoreceptor inner fibers (axons) in the Henle fiber layer,[2–4] in ORT are also reflected externally, wrapping around the surviving cones.[1]

Independently, ORT was designated as a distinctive spectral domain optical coherence tomography (SD-OCT) signature of a thick reflective line surrounding a sometimes extensive and branching

hyporeflective cavity, all within the outer nuclear layer (ONL).[5] A hyperreflective border distinguishes ORT from cysts, which lack this band, in addition to the relative refractoriness of ORT to anti-vascular endothelial growth factor therapy, compared with cysts. Outer retinal tubulation is common in advanced AMD[5–8] and is less common in a variety of other retinal disorders.[5,9–14] Outer retinal tubulation may delimit the border of geographic atrophy (GA) and can be observed overlying fibrotic scars.[7] Outer retinal tubulation is typically found in areas of previous outer retinal damage. Outer retinal tubulation could be described as a response to "death from below," that is, failure of the photoreceptor support system (retinal pigment epithelium [RPE] and choroid) as in choroideremia and some other inherited retinal degenerations.[9,10] Outer retinal tubulation is long lasting[6] and associated with poor visual outcome in anti-vascular endothelial growth factor therapy. Proper recognition of ORT is important clinically for discriminating its presence from ongoing neovascular activity.[5,6,11]

Our goals were to describe histologic characteristics of ORT, identify correlates of known clinical imaging features, and informed and motivated by the histologic findings to seek new imaging features. We especially sought a basis for the reflective ORT border, which previous histology suggested could contain the external limiting membrane (ELM), photoreceptor inner segments, or both. Our results demonstrate the subcellular-level detail available to current generation SD-OCT and provide evidence for an independent reflectivity source in cone inner segments in ORT.

From the *Vitreous Retina Macula Consultants of New York, New York, NY; †Department of Ophthalmology, University of Alabama School of Medicine, Birmingham, AL; and ‡Vision Science Graduate Program, University of Alabama at Birmingham, Birmingham, AL.

Supported by NIH grants EY06109 (C.A.C. and J.D.M.), 5R21EY021903 (Y.Z.), International Retina Research Foundation (Y.Z.), EyeSight Foundation of Alabama (Y.Z.), unrestricted funds to the Department of Ophthalmology from Research to Prevent Blindness, Inc (C.A.C. and Y.Z.), the Vision Science Graduate Program at UAB (K.M.L.), and the Macula Foundation (K.B.F.). Acquisition of donor eyes received additional support from International Retinal Research Foundation, National Eye Institute P30 EY003039, and the Arnold and Mabel Beckman Initiative for Macular Research. Creation of Project MACULA received additional support from the Edward N. and Della L. Thome Memorial Foundation.

K. Bailey Freund is a consultant for Heidelberg Engineering. None of the other authors have any conflicting interests to disclose.

Reprint requests: Christine A. Curcio, PhD, Department of Ophthalmology, EyeSight Foundation of Alabama Vision Research Laboratories, University of Alabama School of Medicine, Room 360, 1670 University Boulevard, Birmingham, AL 35294-0019; e-mail curcio@uab.edu

Methods

This study was approved by the Institutional Review Board at UAB (histology) and the Western Institutional Review Board (imaging) and was compliant with the Health Insurance Portability and Accountability Act.

Histology

We evaluated donor eyes accessioned for research from the Alabama Eye Bank (1995 to 2012) for the presence of ORT. Median death-to-preservation time was 2:40 hours. Eyes were preserved by immersion in 1% paraformaldehyde and 2.5% glutaraldehyde in 0.1 M Sorensen phosphate buffer (pH 7.2) after anterior segment removal. Donor eyes with gross macular appearance consistent with AMD were processed. Tissue was postfixed by osmium tannic acid paraphenylenediamine to accentuate extracellular neutral lipids[15,16] and embedded in epoxy resin (Poly/Bed 812; Polysciences, Warrington, PA). Macula-wide 0.8-μm thick sections[17,18] at 2 mm superior to the foveal center and through the foveola were stained with toluidine blue. Sections were imaged with a ×60 oil immersion objective (numerical aperture = 1.4) and a digital camera (XC10; Olympus, Central Valley, PA). Sections were reviewed in a systematic and unbiased manner.[18] Scanned histologic sections are available online at http://projectmacula.

Eyes containing apparent well-preserved mitochondria were selected for further investigation by transmission electron microscopy (TEM), thin-sectioned at silver-gold, and viewed with a 1200 EXII electron microscope (JEOL USA, Peabody, MA) and an AMTXR-40 camera (Advanced Microscopy Techniques, Danvers, MA). Not all ORT identified by light microscopy were imaged because only one 2-mm region of interest in each 8-mm section fit on a copper grid for TEM. Any ORT in that region was imaged even if not the original ORT of interest. All images were composited with adjustments for exposure, contrast, and background color correction only (Photoshop CS6, Adobe Systems, San Jose, CA).

Spectral Domain Optical Coherence Tomography

Thirty-four patients with known advanced AMD and previously identified ORT were selected. All volume scans for each patient were reviewed to find those of the highest quality. Optical coherence tomography raster scans were acquired with a SD-OCT

system with image averaging (Spectralis; Heidelberg Engineering, Heidelberg, Germany). Because of the retrospective nature of this study, scan pattern (i.e., area covered, number of B-scans, and spacing between adjacent B-scans) varied between patients. Spacing ranged from 11 μm to 242 μm, with the densest scanning pattern (11 μm) showing more detail especially in branching ORT. The presence or absence of a certain ORT finding was recorded and the best-correlated OCT scan selected. Image quality and therefore image information was variable. Scan quality was reduced mostly because of poor fixation, dry eye, and/or cataract.

Nomenclature for the outer retinal hyperreflective bands followed the article by Spaide and Curcio[19] and a recently published proposed lexicon,[20] which included the ELM and inner segment ellipsoid (ISel). As recommended, we subdivided the hyporeflective OCT band commonly called ONL into an outer portion, the anatomical ONL, and an inner portion, the Henle fiber layer.[21,22]

Results

Histology Findings

Forty eyes of 40 donors with neovascular AMD (26 women and 14 men; 85.5 ± 7.1 years) and 13 eyes of 12 donors with GA (9 women and 4 men; 85.7 ± 4.4 years), all nondiabetic white, were reviewed by light microscopy. In 25 of the 40 neovascular AMD eyes (62.5%; 17 women and 4 men; 86.2 ± 6.1 years) and 3 of 13 GA eyes (23.1%; 2 women and 1 man; 86.3 ± 9.6 years), a total of 77 ORT cross-sections were encountered. Of these 77, 65 in sections of good quality and staining were imaged by light microscopy to characterize ORT and generate hypotheses for imaging. From these eyes, 13 neovascular AMD eyes (8 women and 5 men; 84.8 ± 5.4 years) and 1 GA eye (1 man; 77 years) were imaged by TEM, and 30 ORT were identified.

For reference, outer retina in a normal macula is shown (Figures 1A and 2A). The ELM is an interrupted horizontal line of intensely stained junctional complexes between photoreceptor inner segments and Müller cell processes. Processes travel centrifugally within the Henle fiber sublayer of the outer plexiform layer. Müller cell bodies are located in the inner nuclear layer. The ONL has rod and cone nuclei distinguishable by size, chromatin pattern, staining density, and position within the ONL. The inner segments of cone photoreceptors contain pale staining myoids (ISmy), just external to the ELM. Near the outer segment, inner segment ellipsoids (ISel) have darkly stained vertical streaks, representing closely packed thin mitochondria (Figure 2A). Outer segments are recognizable by uniform diameter and staining, with parallel stacked disks.

Cellular ORT constituents are shown in Figures 1–3 and Table 1. An ELM is present at all times and can be considered an ORT requirement. We will refer to 4 histologic phases of photoreceptor degeneration apparent in the lumenal walls of ORT. These cells are radially oriented with respect to the lumen, except where noted. The *nascent* phase exhibits both inner segments and outer segments protruding into the lumen (Figure 1B). The *mature* phase has inner segments only (Figure 1, D and H). The *degenerate* phase has remnant inner segments, no inner segments, or inner segments that are abluminally retracted away from the ELM (Figure 1E). The *end-stage* phase, resembling a funnel in a desolate macula, has no recognizable photoreceptors, just an ELM made by Müller cells (Figure 1F). Robust Müller cell microvilli at the ELM were seen by TEM (Figure 2, B–D). Although cones were the predominant ORT photoreceptor, 4 of 77 (5.2%) of classified ORT had cell bodies consistent with rods (Figure 1D). In ORT, lumens were cells that were nucleated (Figure 1H) and thus presumably capable of gene transcription. Retinal pigment epithelium–derived cells were recognizable by spindle-shaped black melanosomes and green-staining lipofuscin granules (Figure 1, A and G). Non-RPE–derived cells were small (Figure 1G) or medium with heterogenous inclusions typical of macrophages (Figure 2B).

Regarding subcellular constituents, ORT cone inner segment ellipsoids contain mitochondria, recognizable by staining density and texture and confirmed by TEM as reniform organelles containing cristae (Figure 2C). Mitochondria from ORT cones in the *degenerate* phase were sparse and surrounded by a finely granular cytosol lacking other distinctive features or organelles. Abluminally retracted cone cell bodies (Figure 1C) also contained mitochondria (Figure 2C, Figure 3E) as did spheroid cone cell bodies not bordering on the ELM in single sections (not shown). Cone nuclei were always recognizable.

Outer retinal tubulation forms, comparisons with other structures, and formative mechanisms are shown in Figure 3. Outer retinal tubulation is differentiable from cysts, which contain predominantly fluid and lack an ELM and radially oriented surrounding cells (Figure 3A). Also, unlike cysts, ORT is found in closed and open forms (88.3% and 11.1% of classified ORT, respectively). Closed ORT has circular or oval cross-sections, and an ELM border and photoreceptors completely encircle the lumen (Figure 1, A, C–H, Figure 2, B and D, Figure 3A). Closed ORT could

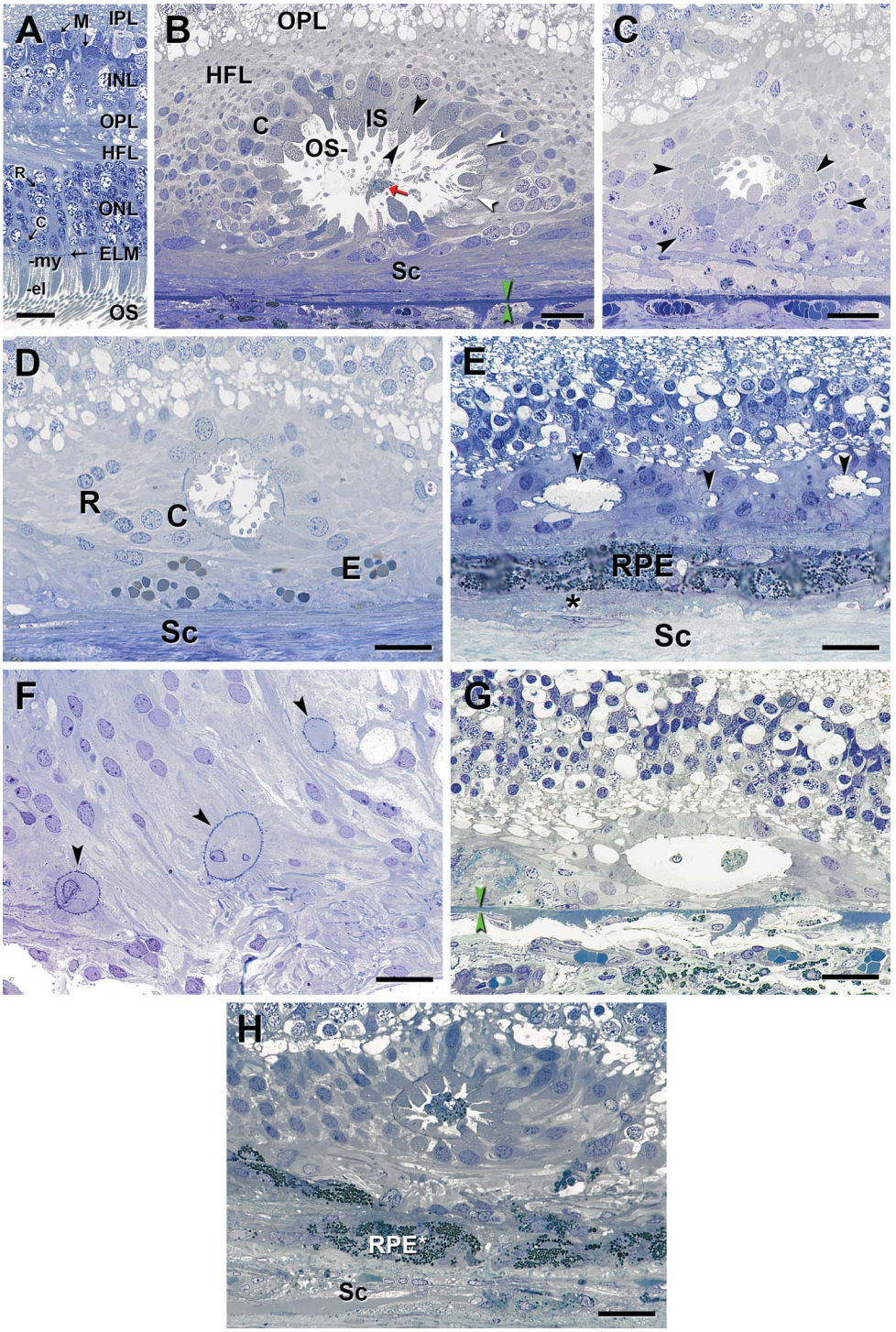

COLOR

Fig. 1. Cellular constituents of ORT in neovascular AMD. Toluidine blue-stained 0.8-μm thick sections of maculas post-fixed by osmium–tannic acid-paraphenylenediamine method. Bars = 25 μm. **A.** Photoreceptors at 2.5 mm temporal to the foveal center in a healthy macula. Rod and cone nuclei are distinguishable by size, chromatin patterns, staining, and position relative to ELM. ISmy (-my) is pale. ISel (-el) has darkly stained vertical streaks indicating closely packed thin mitochondria. M, Müller cell nuclei in the INL. Because of artifactual postmortem detachment, outer segments are bent, en masse, in parallel (85-year-old woman). **B.** Closed ORT: cone nuclei (C) surround a lumen delimited by the ELM (white arrowheads). Cone inner segments, some with outer segments, protrude into the lumen, maintaining a radial organization with respect to the lumen center. Inner segments have mitochondria-containing ellipsoids, and less frequently, myoids (one cell containing both indicated by black arrowheads). One cell with green-staining lipofuscin granules is in the lumen (red arrow). Henle fiber layer contains darkly stained cone fibers in cross-section. Sc, fibrocellular scar. Green arrowheads, Bruch membrane, which is breached in this panel (79 year-old-man). **C.** Cone cell bodies (arrowheads), spheroid in shape, are retracted from the lumen yet contain mitochondria (83-year-old man). **D.** Apparent rod cell bodies (flanking R) and cones (flanking C) in a closed ORT. E, erythrocytes; Sc, fibrocellular scar secondary to CNV (79-year-old man). **E.** Three ORT recognizable by ELM border only (arrows) and lacking inner segments protruding into the lumen; RPE, retinal pigment epithelium; *, persistent basal laminar deposit overlying neocapillaries; Sc, fibrocellular scar subsequent to Type I CNV (82-year-old woman). **F.** Three end-stage ORT (arrowheads). Cells contributing to ELM are all Müller cells, as no photoreceptors survived in this desolate macula (90-year-old woman). **G.** Cells in ORT lumen are RPE-derived with green-staining lipofuscin granules (right) and non–RPE-derived (left) overlying ghost choriocapillaris. Arrowheads, Bruch membrane (80-year-old woman). **H.** Nucleated RPE cell within an ORT lumen; RPE*, RPE-derived cells with spherical melanosomes; Sc, fibrovascular scar (87-year-old man). OPL syn, outer plexiform layer, pedicles, and spherules; HFL, Henle fiber layer (containing photoreceptor and Müller cell fibers); ONL, outer nuclear layer (R = rods, C = cones).

be lined by as few as 3 cones in degenerate phase ($\leq$10 μm diameter, data not shown). Open ORT, in contrast, has horizontally elongated cross-sections, curving ELM at the ends, and nonphotoreceptor cells on the outer aspect (Figure 3, B and E). Asymmetric ORTs are open, with photoreceptors on a lateral

COLOR

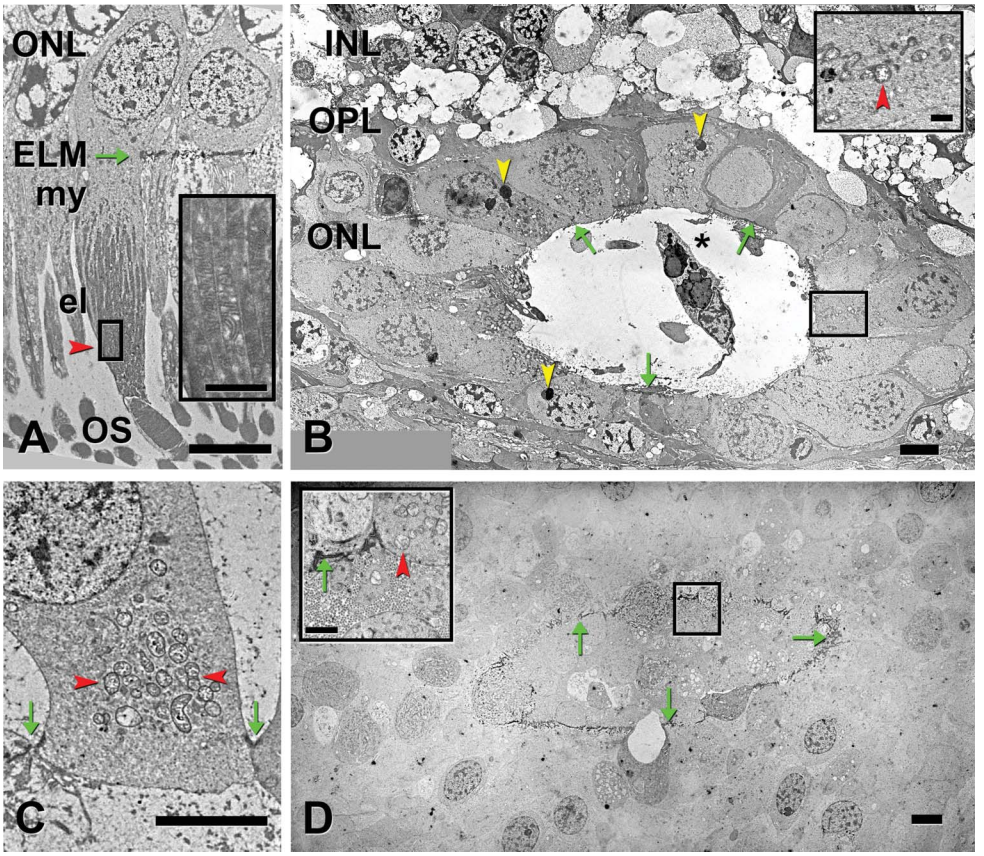

Fig. 2. Subcellular constituents of ORT visible by TEM. Green arrows point to ELM, and red arrowhead point to mitochondria, in all panels. **A.** Photoreceptors at 2.5 mm temporal to the foveal center in a healthy macula. Electron-dense mitochondria (red arrowheads) are thin and tightly packed in the ISel (inset, magnified box) (85-year-old woman). **B.** Degenerate ORT containing macrophage (asterisk) in lumen at 3.2 mm temporal to the foveal center. Mitochondria translocated from ISel to area between ELM (green arrows) and cone nucleus. Cone lipofuscin (yellow arrowheads) are electron-dense granules. Inset, mitochondria in the same photoreceptor on an adjacent section (85-year-old woman). **C.** Cone in ORT showing mitochondria clustered between ELM and nucleus (between red arrowheads); located 3.2 mm from foveal center. **D.** Outer retinal tubulation denoted by continuous ELM containing Müller cell and photoreceptor cross sections; located at 2.4 mm nasal to foveal center. Inset, magnified box of ELM, Müller cell microvilli in cross-section, and mitochondria (79-year-old man). Inset scale bars, 1 μm. Other scale bars, 5 μm.

(Figure 3C) or outer aspect only (not shown). Outer retinal tubulation is lemniscate in cross-section at apparent branch points (Figure 3D). Outer retinal tubulation of all shapes have in common a curved ELM, whereas photoreceptors surviving in islands over fragmented RPE have a flat ELM (Figure 3F). Figure 3, E and G show ORT with multiple phases of cone degeneration in a single cross-section.

Table 1. ORT Correspondences in Histology and OCT

ORT Feature	Histology Figure	OCT Figure
Closed	1B, 1C, 1D, 1E, 1F, 1G, 1H, 2B, 2D, 3A	4A, 4B, 4C, 4D, 4E, 4F, 4H, 5C, 5D, 5E, 5G, 5H, 5K, 5M
Open	3B, 3G, 3D	4C, 5F
Asymmetric	3C	5A, 5B
End-stage	1E, 1F, 1G	Possibly 4B (right); needs scans from earlier in time for certainty
Island	3F	4G
Cyst	3A	4H, 5A, 5B
Flat or ovoid shape	3E	4D, 4E, 5C
Nearby spheroid cones	1C	5B, 5C, 5D
Reflectivity clouds		
Scrolled hyperreflective bands		4H, 5I, 5J
Small cross-section	1E, 1F	4F
Branch	3D	5L, M
Lumenal cells hyperreflective contents	1B, 1G, 1H, 2B	4A, 4D, 4E, 4H, 5G, 5H
Nascent	1B, 3E (left)	
Mature	1D, 1H, 3B, 3C, 3F, 3G (right)	
Degenerate	1C, 1E, 1G, 2B, 3A, 3D, 3E (right), 3G (left)	

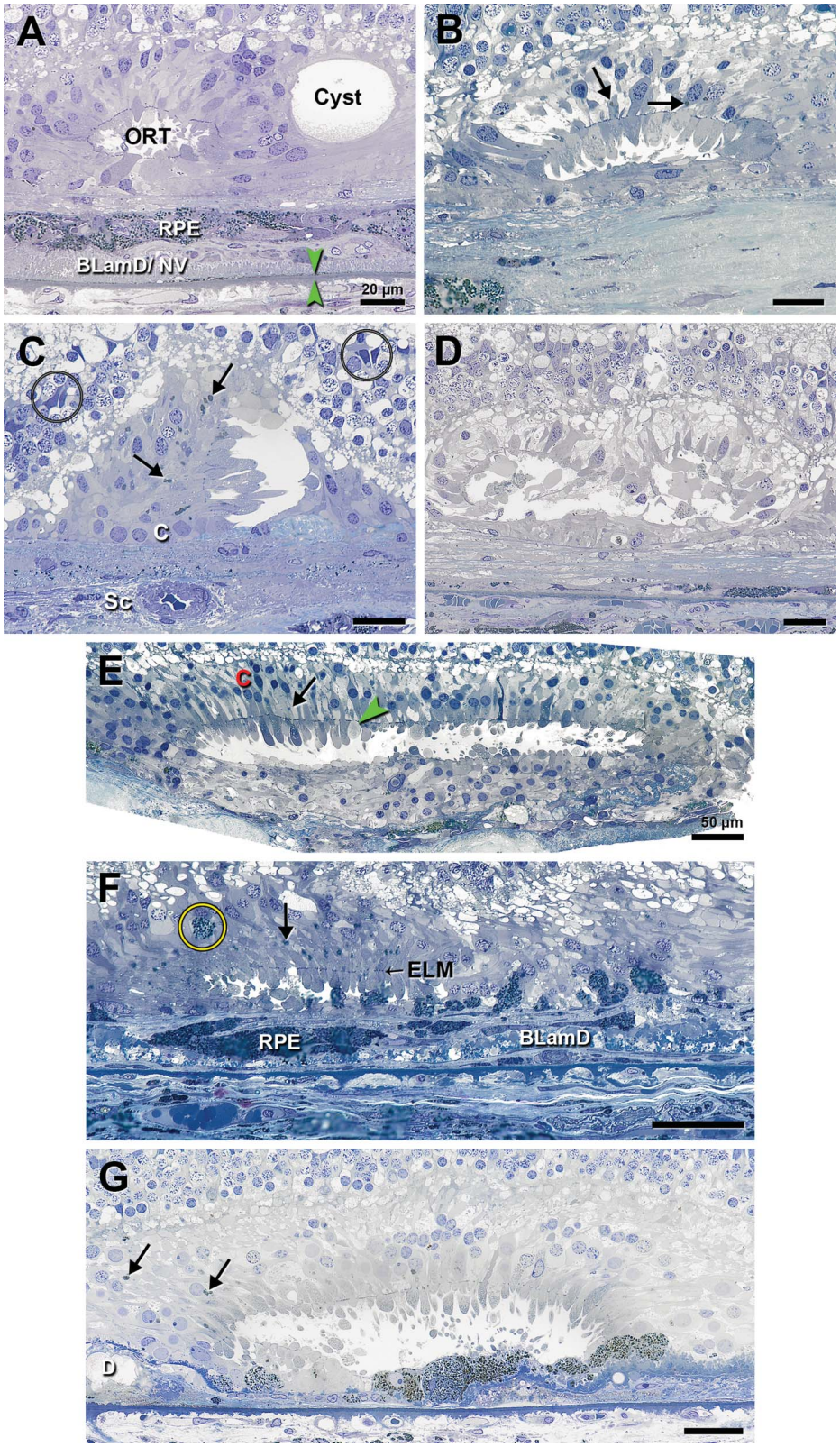

Fig. 3. Outer retinal tubulation forms, differentials, and biogenesis by histology. Neovascular AMD, except where noted. Histologic preparation details and labeling conventions are described in Figure 1. Bars (**A**–**D**), 20 μm; bars (**E**–**G**), 50 μm. **A.** Closed ORT have circular or oval cross-sections, with an ELM border and photoreceptors that completely encircle the lumen. Outer retinal tubulation are distinguishable from cysts, which lack an ELM and an organized arrangement of surrounding cells and contains predominantly fluid. RPE is multilayered and overlies persistent rivulet basal laminar deposits with neovascularization (BLamD/NV). Basal linear deposit is apparent on the surface of Bruch membrane (arrowheads) (87-year-old woman). **B.** Open ORT has horizontally elongated cross-sections, curving ELM at the ends, and an absence of photoreceptors on the outer aspect; arrow, cone lipofuscin (77-year-old woman). **C.** Asymmetric ORT has photoreceptors on a lateral or outer aspect of the lumen only; C, cone nuclei. Müller cell nuclei in inner nuclear layer are circled. Arrows, cone lipofuscin. Sc, fibrovascular scar (79-year-old man). **D.** Open ORT with a lemniscate cross-sectional profile attributed to a branch point. Outer retinal tubulation has various cells in lumen and Müller cells with watery cytoplasm. **E.** Flat closed ORT with cone nuclei (C) and ISel mitochondria, which have retracted inwardly from the ELM (green arrowhead) and from the IS. Spheroid cones have piled up on the outer aspect. Arrow, cone lipofuscin (87-year-old woman). **F.** Surviving island of photoreceptors, not considered an ORT because the ELM (small arrow) is not curved at the ends. Yellow circle, intraretinal RPE; large arrow, cone lipofuscin; RPE, hyperpigmented RPE-derived cells within subretinal fibrocellular scar; BLamD, persistent basal laminar deposit overlying neovascular membrane (94-year-old woman). **G.** An open ORT exhibits different stages of maturity along the lumenal wall, suggesting ORT dynamism. On the right are nearly continuous RPE, inner segments with myoid and ellipsoids, moderately retracted cone nuclei, and remnant outer segments. On the left are RPE fragments, inner segments only with mitochondria retracted behind the ELM, and cone nuclei retracted to a more inward level relative to the right. Persistent basal laminar deposits and neuroglial scar underlie RPE throughout. D, calcified druse. Arrow, cone lipofuscin (87-year-old man with GA).

COLOR

Spectral Domain Optical Coherence Tomography Findings

Outer retinal tubulation was identified in 43 eyes of 34 patients (14 men and 20 women; mean age, 82 ± 12 years) with advanced AMD. Thirty-nine eyes showed neovascular AMD, and 4 eyes had GA. Volumes with closely spaced scans (11 μm) aided the interpretation of features suggested by single-section histology, including groups of spheroid cones, branches, and scrolling of the ELM and ISel bands, by permitting connections to features with secure identity. The subdivision between Henle fiber layer and anatomical ONL could be visualized by tilting the entry beam at the pupil or where these layers were perturbed by pathology in subjacent layers (Figures 4, D and H and Figure 5, J and K).[19,21,22]

Optical coherence tomography findings corresponded well with histologic findings with regard to all features examined (Table 1). Of special interest were ORT definition, differentiation between open and closed ORT, ORT shape, distinction between ORT and cysts, and distinction between ORT and photoreceptor islands (Figure 4). Closed ORT was found in all patients examined (34 patients, 100%), whereas open ORT was found in 14 patients (41%; uncertain in 5 patients, 15%). Asymmetric ORT, hyperreflective "clouds" at a variable distance from ORT, different intralumenal content of ORT, and ORT formation were also correlated (Figure 5). The 4 phases of cone degeneration identified in histology, although hinted at in some OCT scans, could not be reliably identified (Table 1).

Thirty-one patients (91%) had ORT with hyperreflective lumenal content (unclear in 3 patients, 9%). This hyperreflective material was large, circular, and free-floating (4 patients, 13%) or small, dappled, and attached to the hyperreflective border of the ORT (3 patients, 10%), or both (17 patients, 55%). In 7 patients (22%), scan quality did not allow a determination whether intralumenal material was attached or free-floating.

Branching ORT (Figure 5, L and M) was obvious in 20 patients (59%; uncertain in 5 patients, 15%). Asymmetric ORT was found in 9 patients (26%; uncertain in 4 patients, 12%). An area of hyperreflectivity next to an ORT was seen in 12 patients (35%; uncertain in 5 patients, 15%). Photoreceptor islands

COLOR

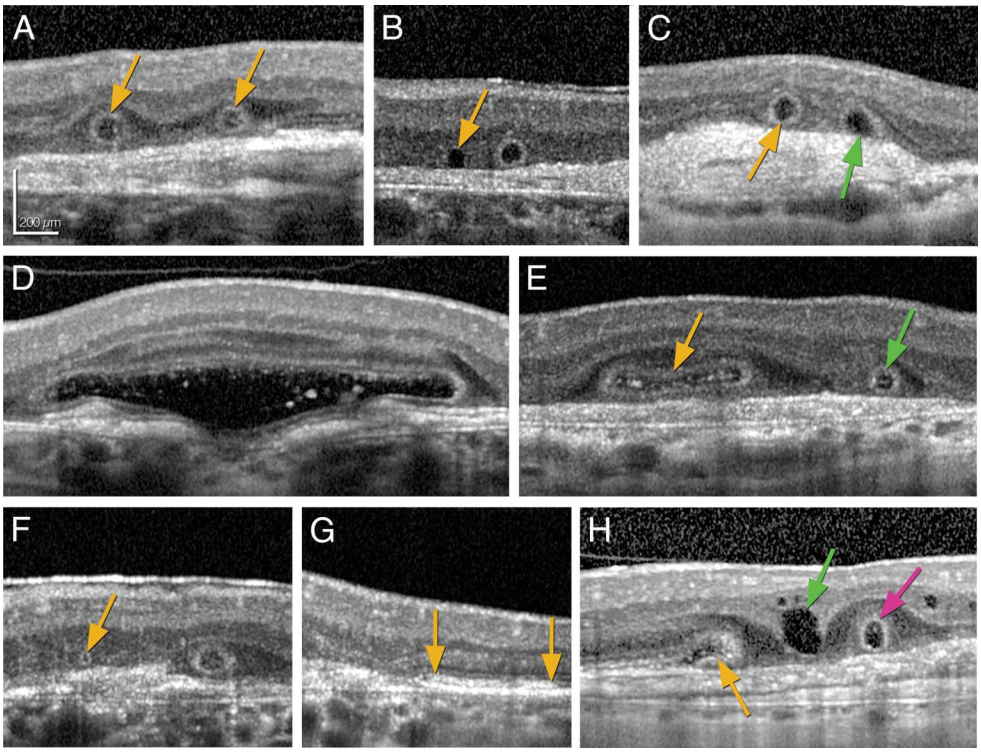

Fig. 4. Outer retinal tubulation shapes and differentials versus other outer retinal structures in advanced AMD. All images were obtained in a Spectralis OCT (with signal averaging). All OCT images are shown in the 1:1 pixel mode for better illustration. **A.** Two circular cross-sections (orange arrows) with internal hyporeflectivity (lumen) and bounded by a thick hyperreflective border located in the ONL overlying a fibrovascular scar. **B.** Next to a circular ORT with a hyperreflective border is a circular cross-section with internal hyporeflectivity lacking a hyperreflective border (orange arrow), which is either a cyst or an end-stage ORT. **C.** A circular cross-section with 360° of hyperreflective border is a closed ORT (orange arrow). An ovoid cross-section lacking hyperreflectivity on its outer aspect (adjacent to the scar) is an open ORT (green arrow). **D.** A large and ovoid cross-section with hyperreflective material attached to the upper part of the hyperreflective border and intralumenal free-floating hyperreflective material (large ORT). **E** and **F.** ORT show different forms. **E.** A flat and ovoid cross-section with a hyperreflective border (orange arrow) has internal hyperreflective material in the lumen. A circular cross-section has a hyperreflective border (green arrow). **F.** A cross section of a very small (42 μm in horizontal diameter) ORT with a hyperreflective border (yellow arrow). **G.** A cross-section showing a preserved hyperreflective band (ellipsoid zone, two orange arrows), where the correct orientation of the photoreceptors and their interdigitation with the RPE is still present (photoreceptor island). **H.** A cross-section showing a forming tubulation (forme fruste ORT) with a free edge to scroll (orange arrow) next to an ovoid cross-section with internal hyporeflectivity lacking a hyperreflective border, located in the outer plexiform layer (cyst, green arrow). Circular cross-section with a thick hyperreflective border (pink arrow) in the ONL (ORT).

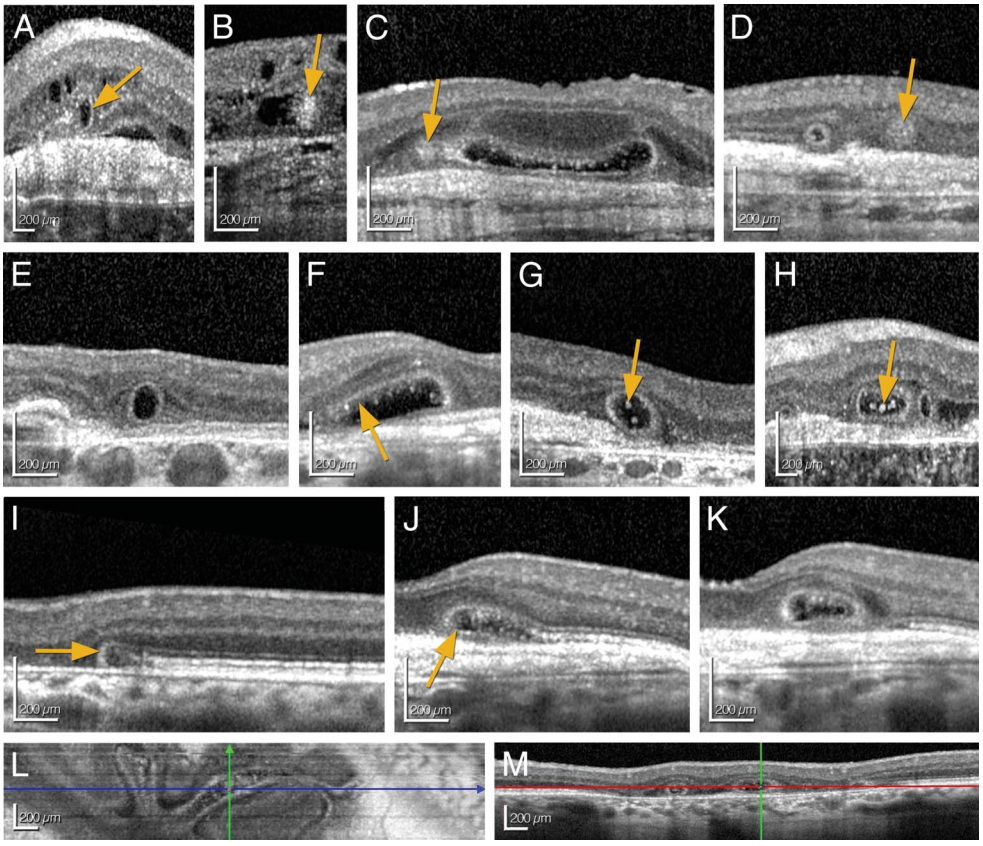

COLOR

Fig. 5. ORT internal contents, associated structures, and formation. **A.** A cross section with a partial hyperreflective line (orange arrow; asymmetric ORT). **B–D.** Cross-sections of well-defined round homogenously hyperreflective clouds (orange arrow) at a variable distance from ORT. **E.** A cross-section with internal hyporeflectivity bordered by a hyperreflective border (no lumenal content). **F.** A cross-section showing hyperreflective material attached to the hyperreflective border at the upper part of the ORT (orange arrow). **G–H.** Cross-sections showing intraluminal free-floating hyperreflective material of different sizes and shapes (orange arrows). **I–K.** Cross sections showing different stages in ORT formation (**J** and **K** are scans 77 μm apart in the same patient). **I.** External limiting membrane circles and thickens (free edge scrolling, orange arrow). **J.** More advanced stage in ORT formation with further scrolling of the free edge (orange arrow) and visibly separating the lumen from the underlying scar by "embedding" the ORT in the ONL. **K.** Circular cross-section of an ORT with a visible 360° hyperreflective band (closed and completely formed ORT). **L.** En face OCT showing ORT branch. Blue line indicates B-scan shown in (**M**). **M.** Scan through the ORT branch shown in (**L**) (two lumen are shown).

were seen in 22 patients (65%; uncertain in 2 patients, 6%). Outer retinal tubulation formation through scrolling from an intact photoreceptor layer (forme fruste ORT) was present in 23 patients (68%; uncertain in 1 patient). The smallest ORT cross-section identifiable in volume scans was 31 μm in diameter.

The reflective ORT border was examined for continuity with normal ISel and ELM bands surrounding the atrophic area. In Figure 5I, the ELM is wider and more reflective, and the ISel is less reflective, at the scroll. We observed reflective material, sometimes continuous like an additional band, internal to and distinct from the ORT border (Figure 4D and Figure 5, C, J, and K). This finding could indicate preserved anatomical ISel.

Discussion

This is the largest number of advanced AMD eyes examined by histology to date specifically for photoreceptor degeneration. A remarkable number of histologic features were found to correspond with OCT features (Table 1). It was possible to identify the ELM and inner segment mitochondria as potential candidates for the reflective border of ORT. Although different eyes were examined clinically and histologically and only morphologic parameters were assessed, the large sample size and numerous correspondences between the two techniques lend credence to our conclusions. One major insight is that although degenerating cones lose outer segments early like degenerating rods, ORT cones, which can survive for extended periods,[6] do so largely without outer segments.

We defined a system of four cone degeneration phases, which in turn directed OCT exploration and identification of four major features of ORT. First, ORT is always located in the ONL, involving both the anatomical ONL and Henle fiber layer, which are not always distinguishable on OCT.[23] Second, on OCT, ORT is defined by a hyperreflective band[5] in closed or open configuration; on histology, ORT is defined by a circular or ovoid ELM border including inner segments in degenerate, mature, and nascent phases and inner segments and outer segments in the nascent phase. Third, the underlying RPE is dysmorphic or absent. Fourth, a "free edge" to scroll seems to be necessary. We do not consider branching a defining

feature because although it is common, not all ORT branch. Groups of spheroid cone cell bodies corresponded to hyperreflective clouds, which were actually glancing sections of ORT that were more apparent on adjacent scans. We found ORT where the ELM seemed to scroll and encircle the photoreceptors (Figure 5, I–K). Optical coherence tomography volume scans revealed a scrolling of the photoreceptor layer that was harder to realize by histology because of limited number of sections. Histology suggests that ORT involutes over time and with the inner segments shrinking and mitochondria migrating through the ELM toward the cone perikaryon. It is important to note that a staging system for cone degeneration is not a staging system for ORT, but rather a necessary first step. An ORT staging system would ideally include measures of how much of each degeneration phase was present, the overall extent of ORT-affected retina, the duration of ORT existence, distances from less affected retina outside the atrophic area, and branching complexity, as complexity likely declines as ORT involutes.

Of the ORT-participating cells, Müller cells seem to be prime movers in formation, apparently sealing off photoreceptors from the RPE–Bruch complex and remaining in end-stage ORT. These findings in AMD parallel long-term experimental retinal detachment.[1,24] Prominence of the persisting ELM (Figure 1F) may be due to selective survival of cytoskeleton-rich plaques on the Müller cell side of ELM adherens junctions as cones die.[25,26] We hypothesize that a requirement for cones and Müller cells with very long processes, found only in the macula, underlies the predilection of ORT for this region. Of interest was the presence of RPE and other cells within the ORT lumen, perhaps providing trophic support to photoreceptors through a connection to less affected retina outside the atrophic area. These cells presumably gain access to the ORT cavity during the scrolling process.

Outer retinal tubulation of AMD can be distinguished from rosettes described in other diseases involving photoreceptors by their tubular structure, large size, and degenerative instead of developmental nature. In tumors affecting young children, rosettes are classified into three types based on the degree of retinal differentiation.[27] Homer Wright rosettes, common in neuroblastoma, contain primitive neuroblastic cells encircling a solid 30-μm to 50-μm diameter central tangle of neural filaments, rather than a lumen.[27] Flexner–Wintersteiner rosettes, common in retinoblastoma, contain early differentiated photoreceptors surrounding a central lumen 40 μm to 60 μm in diameter. Fleurettes are advanced differentiated photoreceptors with inner segments pointing centrally and lacking a lumen. Flexner–Wintersteiner rosettes contain photoreceptors with zonula adherens contacts resembling the ELM, and these cells contain mitochondrial aggregates in inner segment-like compartments.[28] Homer Wright rosettes are arranged in clusters with exclusively circular cross-sections suggesting multiple spheroidal cavities. Outer retinal tubulation is distinguishable from several geometrically diverse malformations, also called rosettes, resulting from ONL dysmorphogenesis in mouse-inherited retinopathies. These include folds with or without internal cells, inward ONL protrusions, and double layers.[29,30] Such malformations are attributed to mislocalization and delayed maturation of photoreceptors and can be associated with defective proteins impacting ELM integrity.[31] Patients with retinitis pigmentosa have rosettes,[32] and rarely, ORT.[10,33] A histologic description of one rosette in such a patient resembles ORT structurally and contains immunohistochemically confirmed rods.[34]

In this first extensive ultrastructural examination of photoreceptor death in human AMD macula, we saw a striking change in cone inner segments mitochondria from long, thin, and bundled to small, ovoid, and dispersed in ORT. Mitochondria are increasingly seen as central to neurodegeneration,[35–43] as well as being essential for oxidative phosphorylation, intermediary metabolism, redox signaling, calcium buffering, and apoptosis regulation. Tightly bundled inner segment mitochondria efficiently use high oxygen from choroid for phototransduction and contribute to inner segment optical properties.[19,44] Mitochondrial morphology is dynamically controlled to respond to energy needs and environmental stimuli by the processes of fusion and fission to form larger and smaller organelles, respectively. Fusion mixes mitochondrial contents and dilutes minimally damaged components among normal organelles. Fission sequesters irreparably damaged components for elimination by mitophagy, a bulk disposal process involving transport toward the soma. Abnormal fusion and fission dynamics contribute to cell death in age-related neurodegenerations such as Parkinson and Alzheimer disease. Images of apparent mitochondrial fission and retraction toward cell bodies in ORT hint at similar processes in human cone photoreceptors degenerating secondarily to support system failure in AMD.

Our observations on ORT add important new information to the debate on the histologic correlate of the second outer retinal hyperreflective band observed with SD-OCT, commonly called the inner/outer segment junction. This name assumes a refractive index boundary at the interface and/or change of the wave-guiding properties between the inner and outer segments of both cone and rods.[45] More recently, this band has been

ascribed to the ISel based on an anatomically correct outer retinal model[19,44,46,47] and corroborated experimentally.[48] As visualized by adaptive optics OCT, the perifoveal ISel band is ~6.0 μm thick, too thick for a single reflective plane, and suggestive of the tapered outer half of the anatomical ISel.[49,50] Comparing OCT scans with histology to test the relative contributions of waveguiding and scattering to band reflectivity has been hindered by the lack of human tissue specimens with perturbed photoreceptor layers, which we here provide.

The optical complexity of ORT is illustrated by the scroll in Figure 5K (also Figure 4D and Figure 5, C and I). The hyperreflective signal closest to the ORT lumen seems stronger when oriented parallel to the RPE. The hyperreflective signal furthest from the lumen, which seems continuous with the ELM, is stronger and wider when oriented orthogonal to the RPE. The poorer transverse (14 μm) versus axial (7 μm) resolution of SD-OCT likely contributes to this difference. While raising many new questions, our current data can support four new concepts about reflectivity sources in OCT. First, ORT cones are radially oriented relative to the ORT lumen and variably oriented relative to the direction of light, making the role of waveguiding in producing the ORT reflective border uncertain. Second, photoreceptors in phases beyond nascent lack outer segments, and thus by definition, lack an inner/outer segment junction, indicating that the reflective border requires neither outer segment nor a junction. However, light scatters back from optical interfaces formed by discontinuities of refractive index, and when outer segment atrophy, new interfaces form between residual inner segments and their surroundings. Third, inner segments have independent reflectivity sources. Because mitochondria occupy ~75% of normal ISel volume,[19] they are obvious candidate scatterers. Mitochondria-associated refractive index gradients may be modulated by metabolic status, organelle shape, and packing within parallel bundles.[44,49,51,52] In ORT, mitochondria alone, among organelles, persist in atrophied inner segments, apparently generating a signal even if shrunken, clustered, dispersed, or randomly oriented. Finally, both the ELM and inner segment mitochondria contribute, although unequally, to the hyperreflective ORT border. Increased hyperreflectivity of the foveal ELM in the absence of hyperreflective cone outer segments occurs early in patients with achromatopsia, a progressive cone degeneration.[53] Because of mitochondrial translocation toward the nucleus in ORT, both structures colocalize within the light path. However, the ELM is normally so small that it must be logarithmically scaled for visibility in SD-OCT B-scans, so the mitochondrial contribution likely dominates.

Whether our hypotheses about ORT reflectivity sources are applicable to normal photoreceptors remains to be determined. A direct continuity of the reflective border of nascent scrolling ORT with the ISel in unaffected retina surrounding atrophy would be definitive, yet such a transition was difficult to discern. It is possible that tilting the OCT light beam within the entrance pupil through directional OCT would reveal photoreceptors that are present but misoriented and thus are poorer waveguides at that critical boundary.[21,22,50] Despite these uncertainties, ISel reflectivity has been used as a measure of mitochondrial health by investigators motivated by the notion that the *ARMS2* gene, a variant of which strongly associates with AMD risk, may encode for a mitochondrial protein.[54] Reduced reflectivity in patients with early AMD was reported.[55,56] The ISel attracts interest because of its correlation with visual acuity and prognostic value in retinal diseases.[57] Defining its correct anatomical substrate thus remains a research priority.

This study had limitations. Different eyes were examined by OCT and histology. The histologic encounter rate is not generalizable to the overall prevalence rate of ORT because these donor eyes were highly selected, and they were accessioned largely before the anti-vascular endothelial growth factor era. The much lower proportion of open ORT in histology relative to OCT may reflect classification uncertainty, advanced state of AMD in these eyes relative to those with active neovascular AMD seen clinically, or both. Histologic analysis used single sections only. Outer retinal tubulation cross-sections are taller on OCT than in histology because of vertical tissue shrinkage during histologic processing and OCT scans vertically stretched for clearer visualization. More ultrastructure from cones at stages between unaffected and entubulated would be useful for testing the mitochondrial reflectivity hypothesis. Additional data from directional OCT and adaptive optics–facilitated retinal imaging could help determine whether cone degeneration phases are visible in vivo. An ORT staging system could be generated in longitudinal studies involving closely spaced SD-OCT volume scans.

In conclusion, ORT demonstrates that photoreceptors have an extended will to live even in advanced AMD. Our data will inform the study of macular cone life and death, mitochondrial dynamics, and concomitant Müller cell activity in clinic populations where high-resolution longitudinal imaging of individual patients is possible. This capability is important

because current animal models of cone degeneration focus on primary neurodegenerations in species lacking long Henle fibers.[58,59] The complementary approaches of histology and clinical OCT can provide important insight into retinal cell biology, tissue optics, and neurodegeneration.

Key words: photoreceptors, Müller cells, age-related macular degeneration, outer retinal tubulation, ellipsoid, reflectivity, optical coherence tomography, histology, transmission electron microscopy.

Acknowledgments

We thank the Alabama Eye Bank for timely retrieval of donor eyes.

References

1. Curcio CA, Medeiros NE, Millican CL. Photoreceptor loss in age-related macular degeneration. Invest Ophthalmol Vis Sci 1996;37:1236–1249.
2. Tsukamoto Y, Masarachia P, Schein SJ, Sterling P. Gap junctions between the pedicles of macaque foveal cones. Vis Res 1992;32:1809–1815.
3. Drasdo N, Millican CL, Katholi CR, Curcio CA. The length of henle fibers in the human retina and a model of ganglion receptive field density in the visual field. Vis Res 2007;47:2901–2911.
4. Polyak SL. The Vertebrate Visual System. Chicago, IL: University of Chicago; 1957.
5. Zweifel SA, Engelbert M, Laud K, et al. Outer retinal tubulation: a novel optical coherence tomography finding. Arch Ophthalmol 2009;127:1596–1602.
6. Jung JJ, Freund KB. Long-term follow-up of outer retinal tubulation documented by eye-tracked and en face spectral-domain optical coherence tomography. Arch Ophthalmol 2012;130:1618–1619.
7. Wolff B, Matet A, Vasseur V, et al. En face OCT imaging for the diagnosis of outer retinal tubulations in age-related macular degeneration. J Ophthalmol 2012;2012:542417.
8. Moussa K, Lee JY, Stinnett SS, Jaffe GJ. Spectral domain optical coherence tomography-determined morphologic predictors of age-related macular degeneration-associated geographic atrophy progression. Retina 2013;33:1590–1599.
9. Goldberg NR, Greenberg JP, Laud K, et al. Outer retinal tubulation in degenerative retinal disorders. Retina 2013;33:1871–1876.
10. Iriyama A, Aihara Y, Yanagi Y. Outer retinal tubulation in inherited retinal degenerative disease. Retina 2013;33:1462–1465.
11. Papastefanou VP, Nogueira V, Hay G, et al. Choroidal naevi complicated by choroidal neovascular membrane and outer retinal tubulation. Br J Ophthalmol 2013;97:1014–1019.
12. Fujinami K, Sergouniotis PI, Davidson AE, et al. Clinical and molecular analysis of Stargardt disease with preserved foveal structure and function. Am J Ophthalmol 2013;156:487–501 e1.
13. Sergouniotis PI, Davidson AE, Lenassi E, et al. Retinal structure, function, and molecular pathologic features in gyrate atrophy. Ophthalmology 2012;119:596–605.
14. Ellabban AA, Hangai M, Yamashiro K, et al. Tomographic fundus features in pseudoxanthoma elasticum: comparison with neovascular age-related macular degeneration in Japanese patients. Eye (Lond) 2012;26:1086–1094.
15. Guyton JR, Klemp KF. Ultrastructural discrimination of lipid droplets and vesicles in atherosclerosis: value of osmium-thiocarbohydrazide-osmium and tannic acid-paraphenylenediamine techniques. J Histochem Cytochem 1988;36:1319–1328.
16. Curcio CA, Millican CL, Bailey T, Kruth HS. Accumulation of cholesterol with age in human Bruch's membrane. Invest Ophthalmol Vis Sci 2001;42:265–274.
17. Curcio CA, Messinger JD, Sloan KR, et al. Human chorioretinal layer thicknesses measured in macula-wide, high-resolution histologic sections. Invest Ophthalmol Vis Sci 2011;52:3943–3954.
18. Curcio CA, Messinger JD, Sloan KR, et al. Subretinal drusenoid deposits in non-neovascular age-related macular degeneration: morphology, prevalence, topography, and biogenesis model. Retina 2013;33:265–276.
19. Spaide RF, Curcio CA. Anatomical correlates to the bands seen in the outer retina by optical coherence tomography: literature review and model. Retina 2011;31:1609–1619.
20. Staurenghi G, Sadda S, Chakravarthy U, et al. Proposed lexicon for anatomic landmarks in normal posterior segment spectral-domain optical coherence tomography: the IN OCT consensus. Ophthalmology 2014;121:1572–1578.
21. Lujan BJ, Roorda A, Knighton RW, Carroll J. Revealing Henle's fiber layer using spectral domain optical coherence tomography. Invest Ophthalmol Vis Sci 2011;52:1486–1492.
22. Mrejen S, Gallego-Pinazo R, Freund KB, Paques M. Recognition of Henle's fiber layer on OCT images. Ophthalmology 2013;120:e32–33.e1.
23. Otani T, Yamaguchi Y, Kishi S. Improved visualization of Henle fiber layer by changing the measurement beam angle on optical coherence tomography. Retina 2011;31:497–501.
24. Anderson DH, Guerin CJ, Erickson PA, et al. Morphological recovery in the reattached retina. Invest Ophthalmol Vis Sci 1986;27:168–183.
25. Williams DS, Arikawa K, Paallysaho T. Cytoskeletal components of the adherens junctions between the photoreceptors and the supportive Muller cells. J Comp Neurol 1990;295:155–164.
26. Omri S, Omri B, Savoldelli M, et al. The outer limiting membrane (OLM) revisited: clinical implications. Clin Ophthalmol 2010;4:183–195.
27. Eagle RC Jr. The pathology of ocular cancer. Eye (Lond) 2013;27:128–136.
28. Ts'o MO, Fine BS, Zimmerman LE. The Flexner-Wintersteiner rosettes in retinoblastoma. Arch Pathol 1969;88:664–671.
29. Fischer MD, Huber G, Beck SC, et al. Noninvasive, in vivo assessment of mouse retinal structure using optical coherence tomography. PLoS One 2009;4:e7507.
30. Stuck MW, Conley SM, Naash MI. Defects in the outer limiting membrane are associated with rosette development in the Nrl-/- retina. PLoS One 2012;7:e32484.
31. van de Pavert SA, Kantardzhieva A, Malysheva A, et al. Crumbs homologue 1 is required for maintenance of photoreceptor cell polarization and adhesion during light exposure. J Cell Sci 2004;117:4169–4177.
32. Milam AH, Jacobson SG. Photoreceptor rosettes with blue cone opsin immunoreactivity in retinitis pigmentosa. Ophthalmology 1990;97:1620–1631.

33. Goldberg NR, Greenberg JP, Laud K, et al. Outer retinal tubulation in degenerative retinal disorders. Retina 2013;33: 1871–1876.
34. Tulvatana W, Adamian M, Berson EL, Dryja TP. Photoreceptor rosettes in autosomal dominant retinitis pigmentosa with reduced penetrance. Arch Ophthalmol 1999;117:399–402.
35. McInnes J. Insights on altered mitochondrial function and dynamics in the pathogenesis of neurodegeneration. Transl Neurodegener 2013;2:12.
36. Maresca A, la Morgia C, Caporali L, et al. The optic nerve: a "mito-window" on mitochondrial neurodegeneration. Mol Cell Neurosci 2013;55:62–76.
37. Youle RJ, van der Bliek AM. Mitochondrial fission, fusion, and stress. Science 2012;337:1062–1065.
38. Federico A, Cardaioli E, Da Pozzo P, et al. Mitochondria, oxidative stress and neurodegeneration. J Neurol Sci 2012; 322:254–262.
39. Chen H, Chan DC. Critical dependence of neurons on mitochondrial dynamics. Curr Opin Cell Biol 2006;18: 453–459.
40. Chen H, Chan DC. Mitochondrial dynamics–fusion, fission, movement, and mitophagy–in neurodegenerative diseases. Hum Mol Genet 2009;18:R169–R176.
41. Knott AB, Perkins G, Schwarzenbacher R, Bossy-Wetzel E. Mitochondrial fragmentation in neurodegeneration. Nat Rev Neurosci 2008;9:505–518.
42. Bossy-Wetzel E, Barsoum MJ, Godzik A, et al. Mitochondrial fission in apoptosis, neurodegeneration and aging. Curr Opin Cell Biol 2003;15:706–716.
43. MacAskill AF, Kittler JT. Control of mitochondrial transport and localization in neurons. Trends Cell Biol 2010;20: 102–112.
44. Hoang QV, Linsenmeier RA, Chung CK, Curcio CA. Photoreceptor inner segments in monkey and human retina: mitochondrial density, optics, and regional variation. Vis Neurosci 2002;19:395–407.
45. Hood DC, Zhang X, Ramachandran R, et al. The inner segment/outer segment border seen on optical coherence tomography is less intense in patients with diminished cone function. Invest Ophthalmol Vis Sci 2011;52:9703–9709.
46. Fernandez EJ, Hermann B, Povazay B, et al. Ultrahigh resolution optical coherence tomography and pancorrection for cellular imaging of the living human retina. Opt Express 2008;16:11083–11094.
47. Huang Y, Cideciyan AV, Papastergiou GI, et al. Relation of optical coherence tomography to microanatomy in normal and rd chickens. Invest Ophthalmol Vis Sci 1998;39:2405–2416.
48. Lu RW, Curcio CA, Zhang Y, et al. Investigation of the hyperreflective inner/outer segment band in optical coherence tomography of living frog retina. J Biomed Opt 2012;17:060504.
49. Meadway A, Girkin CA, Zhang Y. A dual-modal retinal imaging system with adaptive optics. Opt Express 2013;21: 29792–29807.
50. Panorgias A, Zawadzki RJ, Capps AG, et al. Multimodal assessment of microscopic morphology and retinal function in patients with geographic atrophy. Invest Ophthalmol Vis Sci 2013;54:4372–4384.
51. Wilson JD, Cottrell WJ, Foster TH. Index-of-refraction-dependent subcellular light scattering observed with organelle-specific dyes. J Biomed Opt 2007;12:014010.
52. Tychinsky V. The metabolic component of cellular refractivity and its importance for optical cytometry. J Biophotonics 2009; 2:494–504.
53. Greenberg JP, Sherman J, Zweifel SA, et al. Spectral-domain optical coherence tomography staging and autofluorescence imaging in achromatopsia. JAMA Ophthalmol 2014;132: 437–445.
54. Fritsche LG, Loenhardt T, Janssen A, et al. Age-related macular degeneration is associated with an unstable ARMS2 (LOC387715) mRNA. Nat Genet 2008;40:892–896.
55. Wu Z, Ayton LN, Guymer RH, Luu CD. Second reflective band intensity in age-related macular degeneration. Ophthalmology 2013;120:1307–1308.e1.
56. Wu Z, Ayton LN, Guymer RH, Luu CD. Relationship between the second reflective band on optical coherence tomography and multifocal electroretinography in age-related macular degeneration. Invest Ophthalmol Vis Sci 2013;54:2800–2806.
57. Wong IY, Iu LP, Koizumi H, Lai WW. The inner segment/outer segment junction: what have we learnt so far? Curr Opin Ophthalmol 2012;23:210–218.
58. Xu J, Morris L, Thapa A, et al. cGMP accumulation causes photoreceptor degeneration in CNG channel deficiency: evidence of cGMP cytotoxicity independently of enhanced CNG channel function. J Neurosci 2013;33:14939–14948.
59. Ding XQ, Harry CS, Umino Y, et al. Impaired cone function and cone degeneration resulting from CNGB3 deficiency: down-regulation of CNGA3 biosynthesis as a potential mechanism. Hum Mol Genet 2009;18:4770–4780.